Journal of Atmospheric and Terrestrial Physics, Vol. 47, No. 1–3, pp. 159–172, 1985.
Printed in Great Britain.

0021-9169/85 $3.00 + .00

Density and temperature structure over northern Europe

C. R. PHILBRICK
Air Force Geophysics Laboratory, Hanscom AFB, MA 01731, U.S.A.

F. J. SCHMIDLIN
NASA Goddard Space Flight Center, Wallops Flight Facility, Wallops Island, VA 23337, U.S.A.

K. U. GROSSMANN, G. LANGE, D. OFFERMANN
University of Wuppertal, D-5600 Wuppertal 1, F.R.G.

K. D. BAKER
Utah State University, Logan, UT 84322, U.S.A.

D. KRANKOWSKY
Max-Planck-Institut fur Kernphysik, D-6900 Heidelberg, F.R.G.

and

U. VON ZAHN
University of Bonn, D-5300, Bonn, F.R.G.

(*Received for publication* 29 *August* 1984)

Abstract—During the Energy Budget Campaign, a number of profiles of the density and temperature were obtained to study the structure and variability of the atmosphere. The measurements were made using rocket-borne instrumentation launched from Esrange, Sweden, and Andøya Rocket Range, Norway, during November and December 1980. The techniques included meteorological temperature sondes, passive falling spheres, accelerometer instrumented falling spheres, density gauges, mass spectrometers and infrared emission experiments. The instruments provided data covering the altitude range from 20 to 150 km. The measurements were made during periods which have been grouped into three categories by level of geomagnetic activity. Analysis has been made to compare the results and to examine the wave features and variations in the vertical profiles for scales ranging between hundreds of meters and tens of kilometers. Most of the features observed fit qualitatively within the range expected for internal gravity waves. However, the features in the profiles during one of the measurement periods are unusual and may be due to aurorally generated shock waves. The geomagnetic storm conditions caused temperature increases in the lower thermosphere which maximized in the 120–140 km region.

1. INTRODUCTION

An overview of the Energy Budget Campaign has been described by OFFERMANN (1985). One of the objectives of the campaign was to measure the density and temperature profiles in the middle and upper atmosphere during the periods which corresponded to major geomagnetic storm conditions (salvo A), moderate geomagnetic storm conditions (salvo B) and quiet geomagnetic conditions (salvo C). Measurement of the structure profiles provides information on the dynamical response of the atmosphere to the energy deposition during geomagnetically active periods. Many different sensors were used to measure the parameters which are important to understand the coupling between the magnetosphere, ionosphere and neutral atmosphere during disturbed conditions. The criteria for the launch conditions and the overall success of the measurements have been described (OFFERMANN and THRANE, 1981). The enhanced geomagnetic conditions for salvo A were split into two parts, referred to as salvoes A1 and A2. During salvo A1 the measurements were primarily made with payloads launched at Andøya Rocket Range on 27/28 November 1980, while the salvo A2 results were obtained at Esrange on 30 November/1 December 1980. The geomagnetic conditions were nearly identical during salvoes A1 and A2. Table 1 lists the payloads which provided measurements of density and temperature structure during the campaign.

The datasonde consists primarily of a bead thermistor sensor which floats on a starute parachute

Table 1. Measurements during the Energy Budget Campaign which provided information on the density and temperature structure

Date	Time	Site	Salvo	Measurement	Range (km)
7 Nov	2200	Esrange		Datasonde	23–70
7 Nov	2250	Esrange		Passive sphere	44–57
10 Nov	0010	Esrange		Datasonde	29–70
10 Nov	0218	Esrange		Passive sphere	45–87
10 Nov	2200	Esrange	C	Datasonde	23–70
10 Nov	2346	Esrange	C	Passive sphere	32–87*
11 Nov	0012	Andøya	C	Mass spectrometer	95–124
11 Nov	0012	Andøya	C	Density gauge	88–110
11 Nov	0155	Esrange	C	Passive sphere	40–90
11 Nov	0226	Esrange	C	Datasonde	23–70
12 Nov	0020	Esrange		Datasonde	23–70*
12 Nov	0107	Esrange		Passive sphere	33–90
16 Nov	0313	Esrange	B	Infrared spectrometer	60–150
16 Nov	0316	Andøya	B	Infrared photometer	60–150
16 Nov	0331	Andøya	B	Mass spectrometer	100–124
16 Nov	0331	Andøya	B	Density gauge	84–110
16 Nov	0447	Esrange	B	Accelerometer sphere	52–140
16 Nov	0512	Esrange	B	Passive sphere	33–73
16 Nov	0633	Esrange	B	Datasonde	23–70
16 Nov	0751	Esrange	B	Passive sphere	38–90
16 Nov	0823	Esrange	B	Datasonde	23–70
27 Nov	2245	Esrange	A1	Datasonde	23–70
28 Nov	0047	Esrange	A1	Passive sphere	40–88
28 Nov	0325	Andøya	A1	Density gauge	86–102
28 Nov	0329	Esrange	A1	Passive sphere	35–90
28 Nov	0419	Esrange	A1	Datasonde	30–60
1 Dec	0009	Esrange	A2	Accelerometer sphere	55–150
1 Dec	0024	Esrange	A2	Passive sphere	32–61
1 Dec	0139	Esrange	A2	Passive sphere	41–87
1 Dec	0233	Esrange	A2	Datasonde	30–70

* Significant gaps exist in the data profile within the given range.

after release from a small rocket payload. These sondes are the standard meteorological sensors for measurements of temperature and wind between 20 and 70 km (SCHMIDLIN, 1981). Significant corrections must be applied in the analysis of the higher altitude data and, therefore, the errors grow rapidly above 60 km. Since all of these measurements were conducted at night, the radiation corrections are small and the measurements should be useful over the reported altitude range. The density profile is determined by use of the hydrostatic equation and requires a low altitude normalization to another technique, either rawinsonde balloon or pressure map analysis.

The passive sphere, a one-meter metalized mylar inflated sphere, is released at altitudes above 100 km and tracked by a precision radar to provide acceleration components (ENGLER, 1965; QUIROZ and GELMAN, 1975; PHILBRICK *et al.*, 1978b). The DFVLR MPS-36 radar measured the position and velocity components used to determine altitude and horizontal wind velocities. The derivatives of the position and velocity are used to derive drag acceleration and determine the atmospheric density. The density profile is integrated downward to determine the temperature using the hydrostatic equation, the ideal gas law and an assumed upper level temperature point. The initial temperature to start the calculation may be chosen from any model value. By the time the equation has been integrated over about one and one-half scale heights (about 10 km), the sensitivity of the result to the initial estimate is negligibly small. The hydrostatic equation

$$dP = -\rho g\, dZ \tag{1}$$

can be combined with the ideal gas law

$$P = \rho RT/M \tag{2}$$

to yield the differential equation

$$-(M/R)g\rho\, dZ = d(\rho T). \tag{3}$$

Integrating equation (3) and rearranging terms yields

an equation

$$T_2 = T_1(\rho_1/\rho_2) - (M/R)g \int_{Z_1}^{Z_2} (\rho/\rho_2)\, dZ, \qquad (4)$$

which is strongly convergent when used to integrate downward from some assumed initial value T_1 along the density profile $\rho(Z)$. The passive sphere gives the opportunity to obtain a significant number of profiles for density, temperature and wind because it is a relatively inexpensive technique. Measurements are generally useful over the altitude range 30–90 km. The results are calculated directly from the first and second derivatives of the range and angle data to obtain velocity and acceleration components. All of the results depend upon the accuracy of the radar track and since taking the derivatives tends to accentuate any noise, it is necessary to heavily smooth the measurements at high altitudes. Typical smoothing intervals are about 3 km at 60 km, 6 km at 80 km and 12 km at 90 km altitude. From prior studies of the errors introduction by smoothing the radar data (PHILBRICK *et al.*, 1978b), particular care must be given to the interpretation of the profiles and their wave features above about 78 km.

Density gauge measurements were obtained using a miniature hot filament ionization sensor on three rocket payloads launched from Andøya. The density gauge is of a nearly open flow design with capability of measuring in the limited altitude range between 90 and 110 km. The measurements are somewhat difficult to interpret because of the weak shock around the vehicle over most of the measurement range. The results were found to be in general agreement with those presented herein, but do not add significantly to the present description.

A temperature profile was also obtained from the infrared spectrometer measurements of the CO_2 15 μm emission. To derive the temperature profile, the theoretical spectra of the 15 μm band were calculated using the AFGL Atmospheric Line Parameters Compilation tape (MCCLATCHEY *et al.*, 1973; ROTHMAN, 1981). The reabsorption of radiation was taken into account by solving the radiative transfer equation for each individual line. The density of the CO_2 was obtained by multiplying the measured total density by 330 ppm, but the emission is much more dependent upon temperature than the small error in this computation of CO_2 density. The theoretically calculated intensities were fitted to the measured intensity profile with temperature as a free parameter. The resulting temperature profile depends upon the implicit assumption of local thermodynamic equilibrium, which condition should be the case for altitudes up to the vicinity of 80 km. Above 80 km the derived temperature reflects the excitation temperature of the CO_2. During the night the excitation temperature of CO_2 slowly decreases with increasing altitude (KUMER, 1977), independent of local gas-kinetic temperature.

The mass spectrometer measurements of N_2 described by WIRTH and VON ZAHN (1981) have been used to determine temperature profiles based on integration downward along the profile under the assumption of hydrostatic equilibrium. This technique provides high resolution N_2 measurements which have been used to derive a temperature profile between 100 and 125 km by integrating equation (4).

The accelerometer sphere measurements were made using a triaxial piezoelectric accelerometer, which has the advantages of high sensitivity, high vertical resolution and large dynamic range for making measurements (PHILBRICK *et al.*, 1978a; PHILBRICK *et al.*, 1981). The accelerometer directly measures the drag acceleration components which can be used to determine the density from the drag force,

$$ma_D = \tfrac{1}{2}\rho v^2 C_D A, \qquad (5)$$

where the drag coefficient C_D is based on wind tunnel measurements (BAILEY and HIATT, 1972) below 90 km, which transition into free molecular flow values above 120 km (PHILBRICK *et al.*, 1978a). The sphere was released from the rocket near 70 km on up-leg and measurements were made over apogee and down to about 50 km on down-leg. The mass distribution of the sphere was carefully balanced to provide gyroscopic stability, minimize aerodynamic torque and predefine the precession frequency relative to the spin frequency so that electronic filtering could be built into the data system. A beacon transponder was included to provide precision altitude measurements from the tracking radar. The accelerometer is capable of measuring the density, temperature and wind over the altitude range from 50 to 150 km with a vertical resolution of approximately 100 m. In addition to the rocket-borne techniques, the mesopause temperature was monitored by use of ground-based near infrared measurements of the OH emission (LANGE *et al.*, 1981; BAKER *et al.*, 1981). This paper will present an overview of the structure measurements, intercompare the results and infer several points about the response of the atmosphere during the geomagnetic heating periods.

2. RESULTS

The results for the temperature measurements below 90 km altitude are shown in Figs. 1a–d and the density results in Figs. 2a–d. The identification of the various measurement times and salvoes is given in Table 1. The U.S. Standard Atmosphere, 1976 (USSA 76) (COESA,

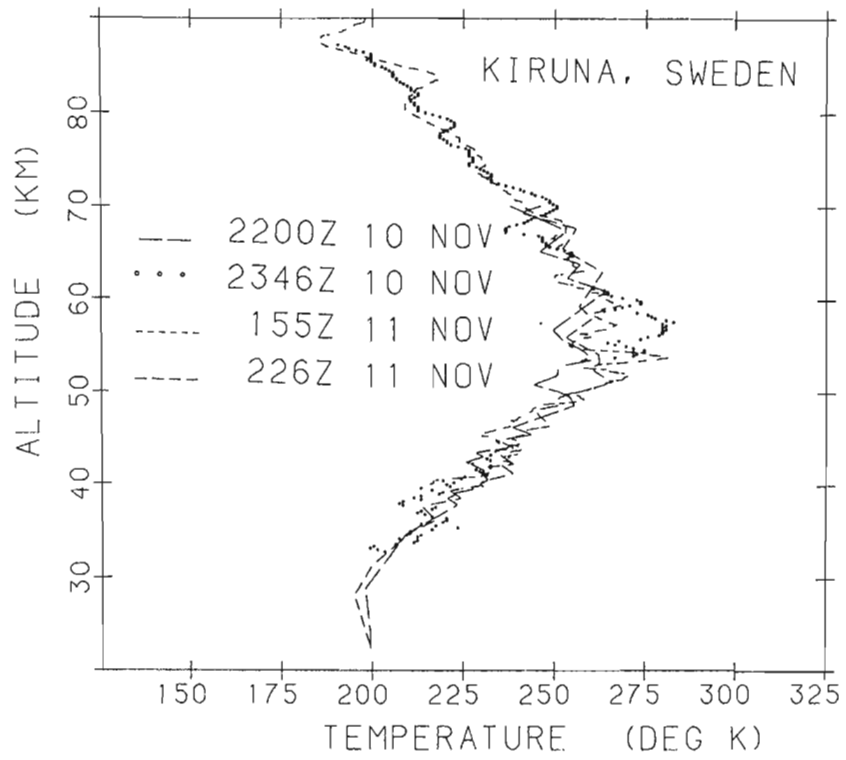

(a)

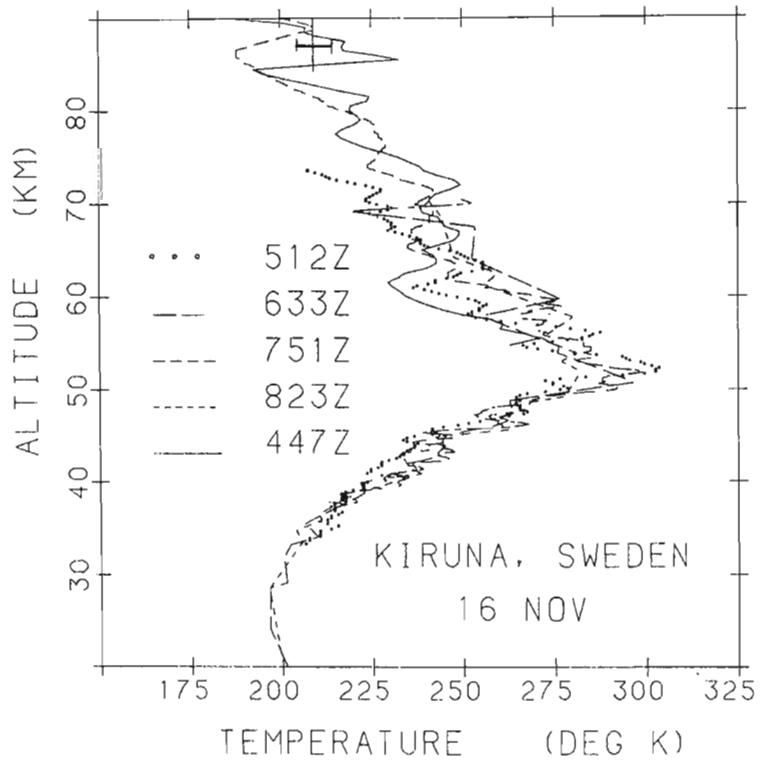

(b)

Fig. 1. Temperature measurements for the altitude range 20–90 km from the various measurement techniques (see Table 1): (a) salvo C; (b) salvo B; (c) salvo A1; (d) salvo A2. The ranges of the OH airglow determination of temperature during salvoes A1, A2 and B are also indicated in the 84–90 km region.

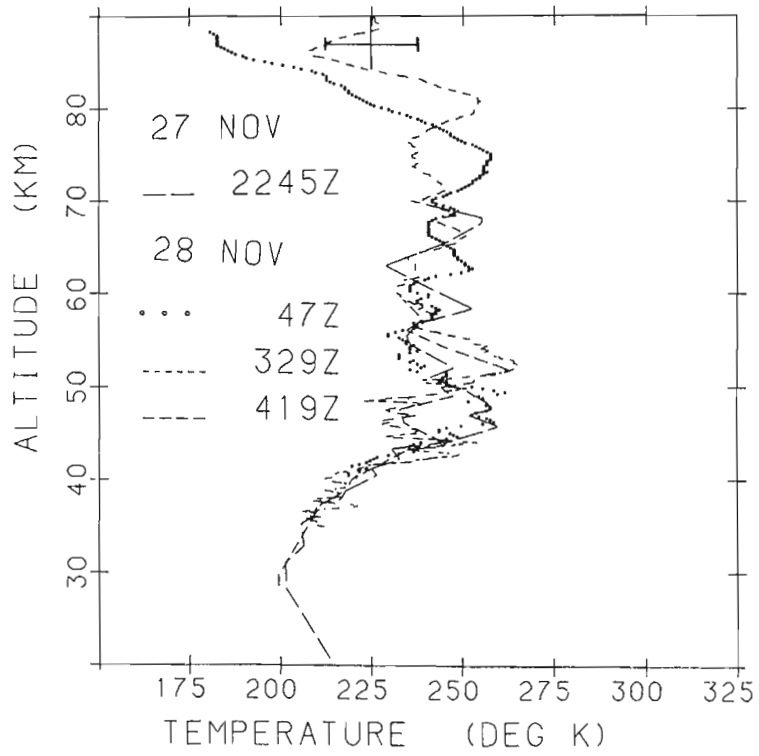

(c)

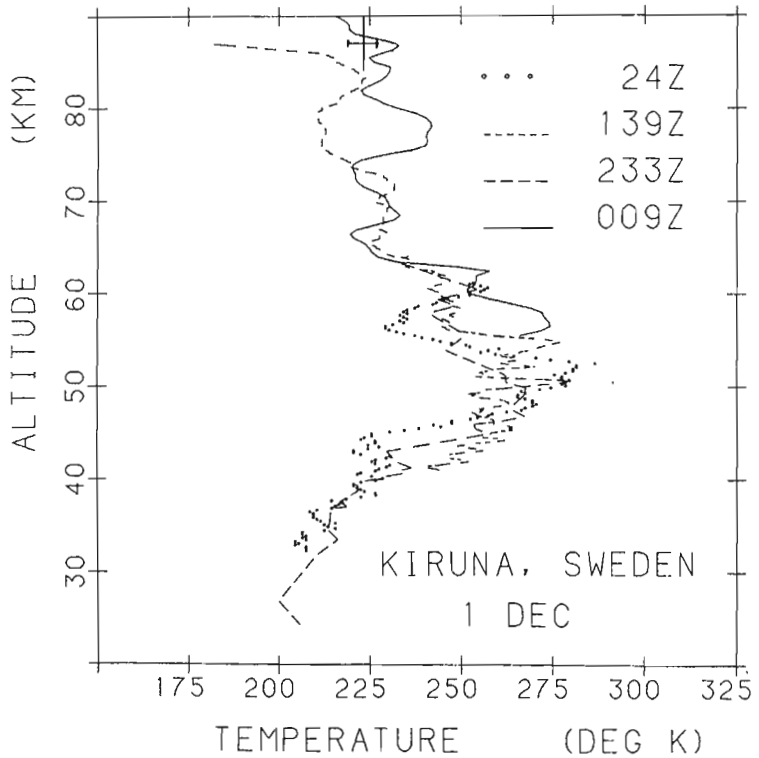

(d)

Fig. 1 continued.

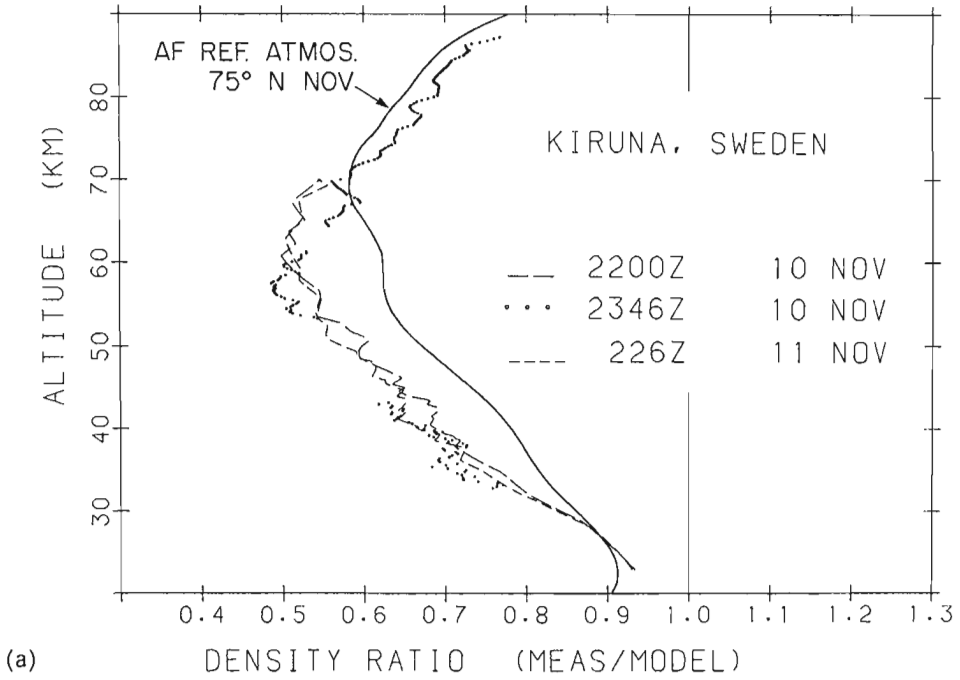

(a)

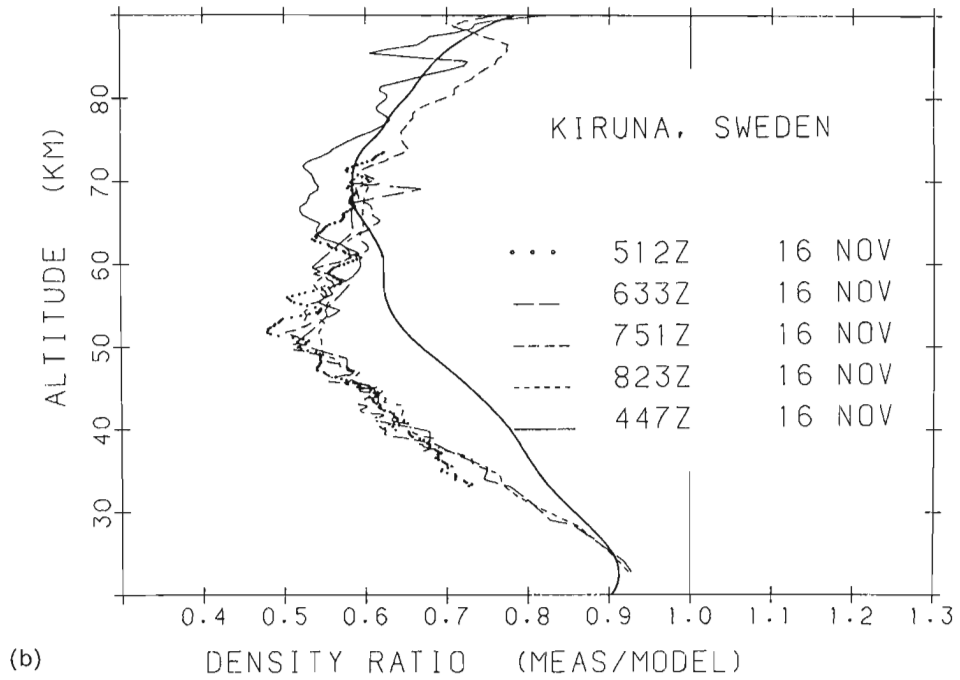

(b)

Fig. 2. Density measurements in the 20–90 km region are shown as a ratio to the USSA 76 model for each of the salvoes: (a) salvo C; (b) salvo B; (c) salvo A1; (d) salvo A2. Refer to Table 1 for identification of the technique used for each measurement. A reference model (November 75°N) is shown to indicate the change in the mean conditions for the season and latitude effects.

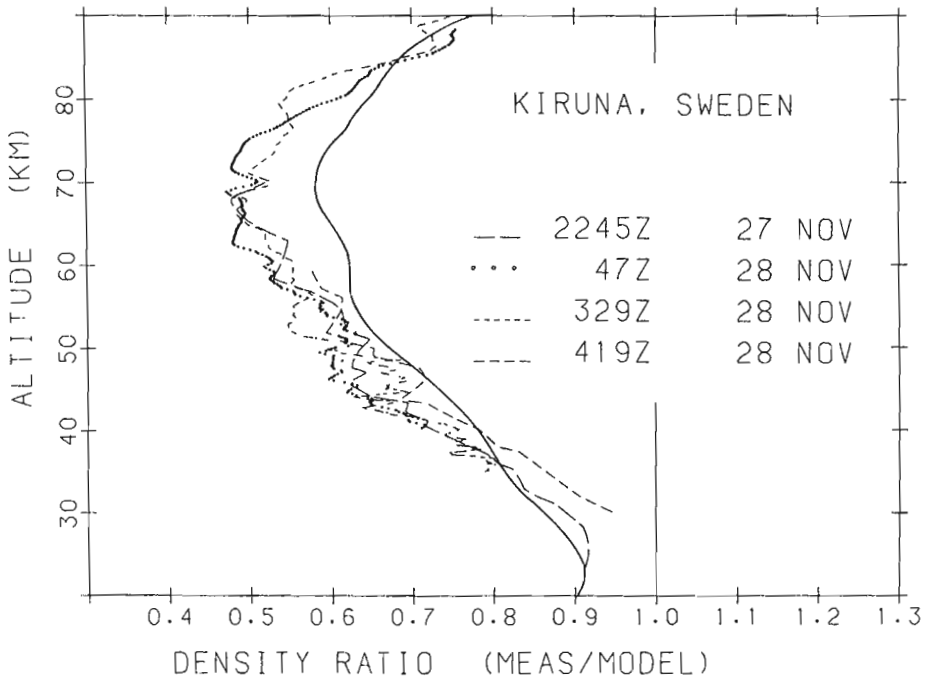

(c)

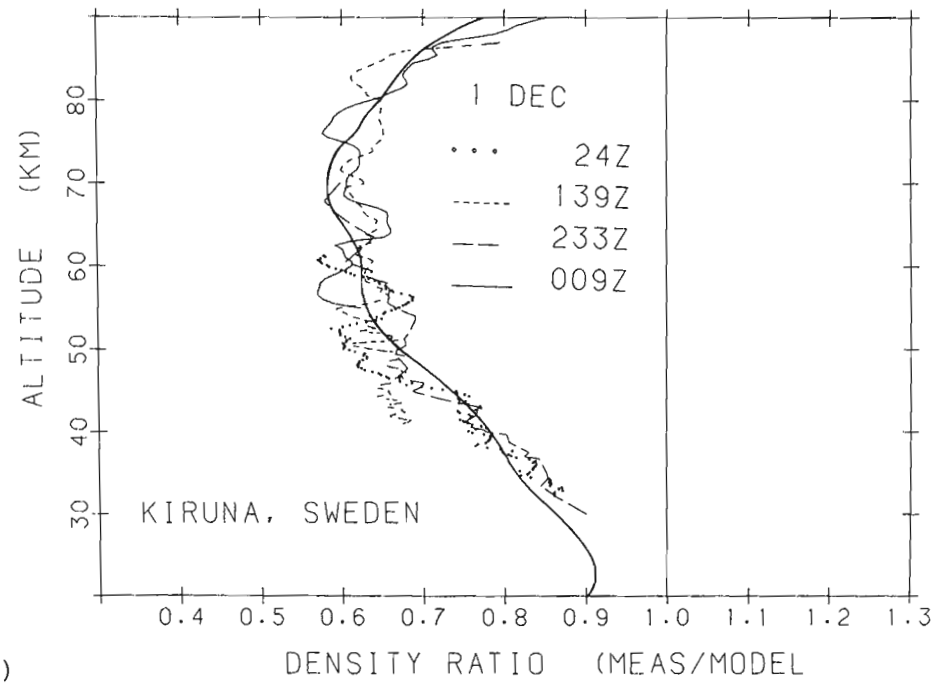

(d)

Fig. 2 continued.

1976) has been chosen as the basis for the density data comparisons. The density profiles are more easily compared when the ratio to such a reference model is presented. The measurements of temperature during the geomagnetically quiet conditions (salvo C) (Fig. 1a) on 10–11 November show excellent agreement between the datasonde and passive sphere results in the regions of data overlap. The general features in the density and temperature profiles are stable over the period of several hours during that night. However, wave activity is present even during this quiet geomagnetic period, with the largest wave amplitudes between 50 and 60 km. The period of the wave activity is comparable to the measurement separation and thus it is not possible to follow the wave behavior. For the background conditions of salvo C, the range of variation in the temperature is less than 20K, except for the stratopause region where differences range to 30K.

In Figs. 1b–d the temperature structures for the geomagnetically active periods are shown. Figs. 1c and d show the temperature results from the University of Wuppertal's ground-based IR spectrometer measurements of OH emission over Esrange during the nights of salvoes A1 and A2. During salvo B, measurements of the temperature from the OH emission were obtained by the Utah State University instrument at Andøya Rocket Range. The measurements from the OH emission temperatures are shown in Figs. 1b–d, with the vertical bar indicating that the emission corresponds to a thick layer near 87 km. The length of the temperature bar corresponds to the range of the variations during the night, not to the error in the technique, which is significantly smaller. Salvo B represents a much more active dynamical condition than any of the other measurement periods of this campaign and the wave-like structure features are much stronger than for any of the other cases. When the various profiles are compared, the period of the wave activity can be estimated for a few altitude ranges where larger features are observed. These cases indicate periods ranging from about 1 to 4 h. The better examples are found at 57 and 52 km in salvo C, at 60 km in salvo B, at 53 and 47 km in salvo A1 and at 56 km in salvo A2. While it is difficult to make the case that the enhanced wave activity during salvoes B, A1 and A2 is due to the increased geomagnetic activity, it may be expected that momentum sources (TRINKS *et al.*, 1979) may couple wave activity into the lower thermosphere, which would propagate into the middle atmosphere with little or no attenuation. Certainly, in the cases of the measurements during this campaign, large amplitude wave features were observed in the mesosphere on nights of enhanced geomagnetic activity which were not present on quiet nights.

A significant difference between the shape of the temperatures profiles measured during salvoes C and B and those measured during salvoes A1 and A2 is observed. The shape of the stratopause mean profile, which is rather peaked for the first two salvoes, is flattened in the last two salvoes. Salvoes A1 and A2 were carried out during periods of higher geomagnetic activity, however, this large change in the overall shape of the temperature profile should probably be associated with a more general change in atmospheric circulation which occurred during the 10 days between salvo B and salvo A1 (LABITZKE and BARNETT, 1985). The winter variability, particularly during periods around stratospheric warmings, is sufficiently well known that several models of winter warmings are available in the AF Reference Atmosphere (COLE and KANTOR, 1978). A comparison of the results of salvo B and salvo A1 with the models for extreme winter conditions of the warm and cold stratosphere, respectively, show close agreement in both magnitude and shape between the measured and modeled profiles.

The density profiles of Fig. 2 are shown relative to the USSA 76 model. The comparison of the density measurements with the AF Reference Atmosphere (COLE and KANTOR, 1978) for 75°N latitude and November conditions is also shown. This comparison demonstrates that the major profile differences between the campaign results and USSA 76 are due to the mean dependence on latitude and season. The range of the density variations on individual nights is less than about 15%, except for differences up to about 25% in salvo B. Significant wave activity is seen in all of the profiles, particularly during the geomagnetically active periods. Similar comments apply to the density variation as to the temperature variation relative to the possible wave features in response to localized heating and momentum coupling. The wavelengths and periods which would be inferred from these results are within the range that would be expected for internal gravity waves in the altitude region of the measurements. Figure 3 shows a convenient guide for comparison of the wave structure observed. The figure follows from the original work of HINES (1974), but has been modified in the manner of his suggestion to include the effects of eddy diffusion (PHILBRICK *et al.*, 1978b) using the profile adopted from the ALADDIN experiments. The figure indicates that the waves from the lower atmosphere of certain horizontal and vertical size, to the right of the short dash lines, will be reflected before reaching the mesosphere. In addition, the amplitude of waves which are below a certain size is quickly lost by viscous dissipation (scales to the left and below the long dash lines) and thus these cannot be a major contributor to mesospheric waves. Figure 3 has

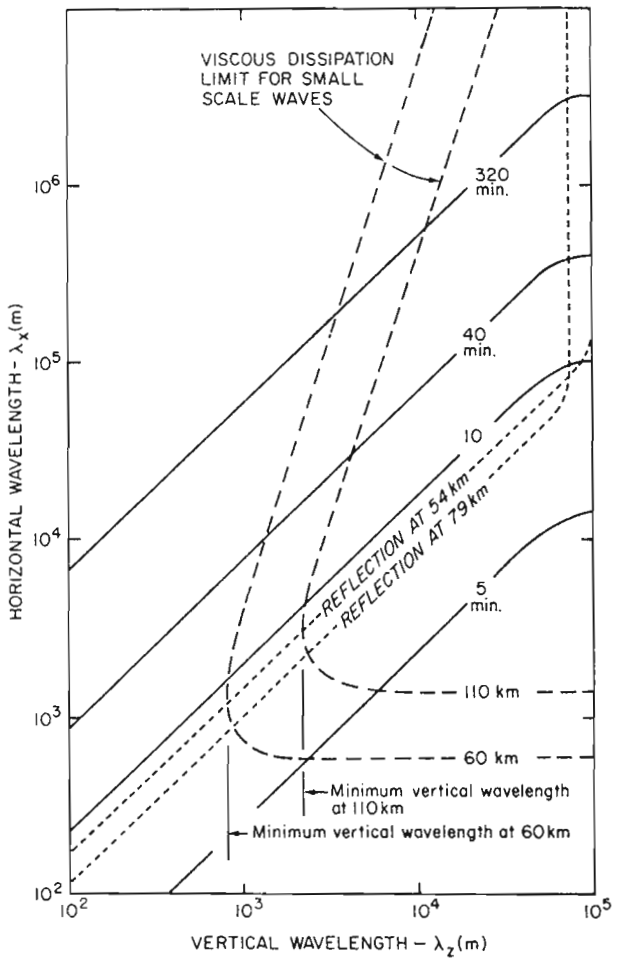

Fig. 3. Wavelengths of propagating modes expected in the mesosphere and lower thermosphere from a re-examination of the analysis of HINES (1974) with inclusion of an eddy viscosity contribution. The periods in minutes are shown as constant period contours (solid lines). The viscous dissipation limits for small-scale waves at 60 and 110 km are shown (dash lines) and represent the limits of the permitted spectrum from effects of viscous damping (modes lying to the left and below these curves are excluded). Modes subject to reflection back toward the ground at heights of 54 and 79 km are indicated (dot lines) and modes lying to the right of these curves are reflected back into the lower atmosphere (PHILBRICK *et al.*, 1978b).

been found to provide a reasonable representation of the scales and periods of wave features found in the mesosphere. The minimum vertical wavelength near 60 km should be approximately 800 m and at 110 km the minimum vertical wavelength should be about 3 km. Most of the cases which can be examined, based upon rocket data obtained in this experiment and several previous investigations, indicate that most frequently, the vertical wavelengths between about 3 and 10 km dominate the wave structure in the mesosphere. Based upon the vertical scales observed and the tendency towards a centroid region within the context of Fig. 3, the corresponding horizontal scales would be expected to range between about 10 and 100 km and corresponding periods between about 15 min and 2 h.

Preliminary results of some of the density and temperature profiles have been reported previously (PHILBRICK *et al.*, 1983). One of the density profiles reported at that time for salvo C (0155Z on 11 November) was consistently higher by about 10% than other flights on the same night over the entire altitude range. That density profile has been omitted from this final analysis because it is believed that an anomalous error in the weight of the sphere system was present. A loss of about 15 g of the fluid used to pressurize the sphere could account for the discrepancy. The temperature profile for the flight has been retained because of the close agreement with the other flights of that night. The suspected change in mass would not effect the temperature because it is only proportional to the density ratio and gradient (see equation 4). However, a loss of mass would result in a slower fall velocity and inferred higher density. Since this preliminary report, corrections to the accelerometer data (measurements at 0447Z on 16 November and 0009Z on 1 December) have been included which account for errors introduced by the preliminary analysis of the trajectory, the orientation of the position of the spin axis in inertial space and a small bias error which had been introduced in analysis of the laboratory calibration data. In addition, this analysis includes a much more detailed calculation of the effect of the rotational inertia lost due to the atmospheric drag below 90 km.

In Fig. 4 the comparison between the temperatures measured by the piezoelectric accelerometer for the salvo B and A2 conditions is shown. Both cases exhibit large wave oscillations in the vertical profile. The results of salvo A2 indicate a significant heated region in the vicinity of 120 km, which is probably due to Joule heating from the strong geomagnetic activity present during this period. The major input of Joule heat energy has generally been considered to be in the altitude region between 120 and 140 km, based on the response of the atmosphere measured at satellite altitudes (PHILBRICK, 1977). A case which should correspond to strong Joule heating (salvo A2) compared to a case which corresponds to strong particle input (salvo B) shows that indeed the temperature between 110 and 140 km is increased. Salvo B corresponded to a case of significantly more energy input from the particle flux (TORKAR *et al.*, 1985), but the energy was primarily dissipated by ionization. The high particle flux energy contributes little to the neutral atmosphere. The energy transfer from electrodynamic heating (COLE, 1971), as this case indicates, has the more significant effect on the thermal structure of the atmosphere.

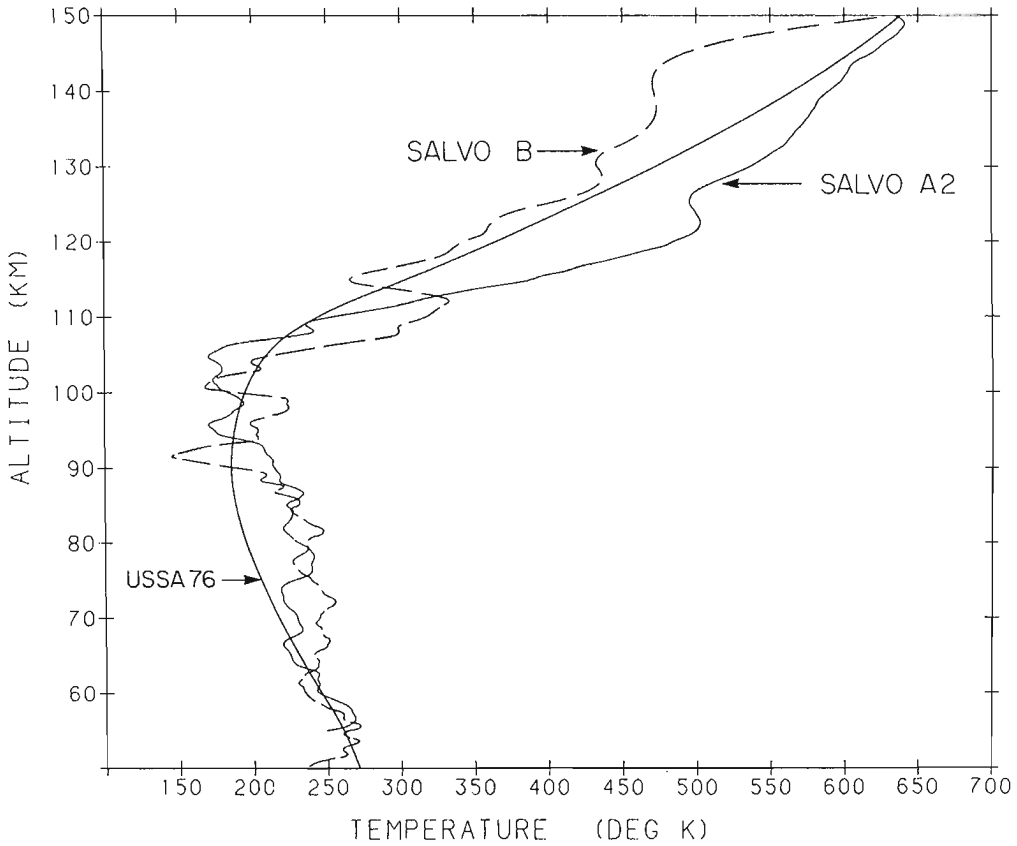

Fig. 4. Temperature profiles determined from the density measurement of the piezoelectric accelerometer during salvo B and salvo A2 show a singificant increase in temperature between 110 and 150 km, which is associated with heating during the period of larger geomagnetic activity. Note that the mesopause appears in the vicinity of 100 km.

Figure 5 shows the temperature profiles obtained during salvoes B and A2 over the altitude range between 30 and 120 km. The profiles obtained from the infrared spectrometer and the mass spectrometer are shown for comparison with the other techniques. The profile at 0331Z on 16 November is from the N_2 measurements of the mass spectrometer. The temperature profile was obtained by integrating down the N_2 density profile using equation 4 from an initial value of 420K at 125 km. The portion of the profile shown between 100 and 113 km is relatively independent of the assumed initial value. While the temperature determined from the IR radiance at 0313Z on 16 November agrees with the other measurements, it should be remembered that the emission becomes decoupled from the local thermodynamic equilibrium for altitudes above 80 km. That profile has been included to the higher altitudes for a relative comparison. The very strong gradients in the temperature profiles from the sphere results lead to questions about the origin and strength of the source which would be responsible for generating such irregularities. Also, the profiles from the IR measurement and the mass spectrometer measurement on the night of 16 November show extremely sharp features in their profiles. Comparison with the results from salvo A2 on 1 December indicate again the unusual character of the salvo B measurements. While salvo A2 does show significant wave activity, the wavelengths and temperature gradients are generally in agreement with the wavelength scales presented in Fig. 3 and with minimum gradients approaching the adiabatic lapse rate (about -10K km^{-1}). [It is worth noting that the mesopause is centered near 100 km for this case, which is generally representative of the mean model winter condition for altitudes below 90 km (see Fig. 2d).] However, the wavelengths and temperature gradients of Fig. 5a are not explainable in the same way. The temperature gradients in several of these regions are super adiabatic. In Fig. 6 the density profile for the accelerometer measurement on 16 November corresponding to the temperatures of Fig. 5a is presented. The profile is quite unusual in that there exist three regions where the gradient of the atmospheric density exceeds the values that could exist in a stable stratified atmosphere, or even acceptable values for a turbulence

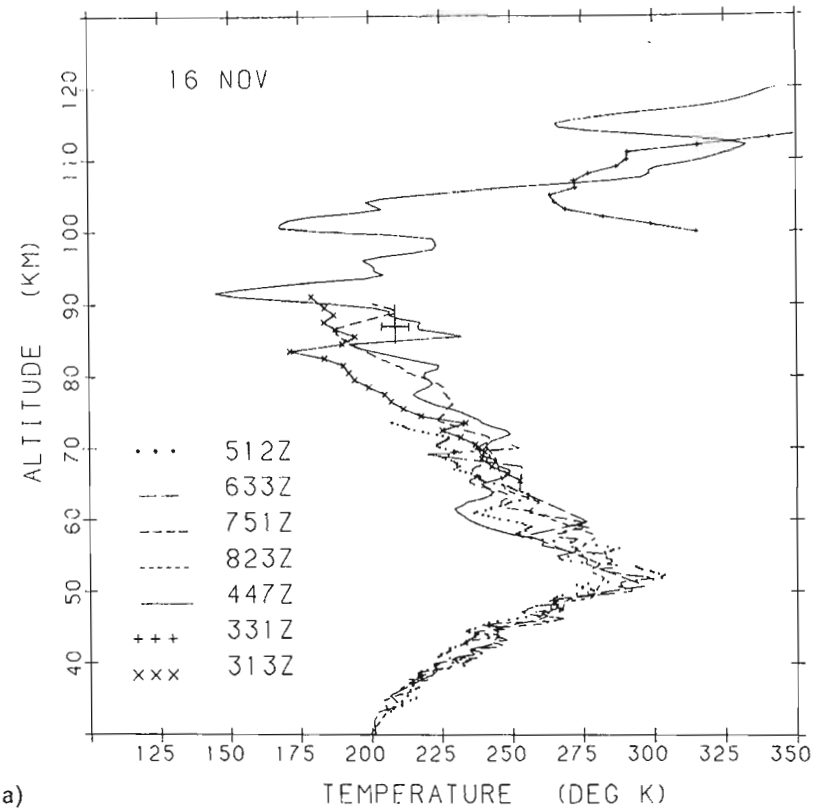

(a)

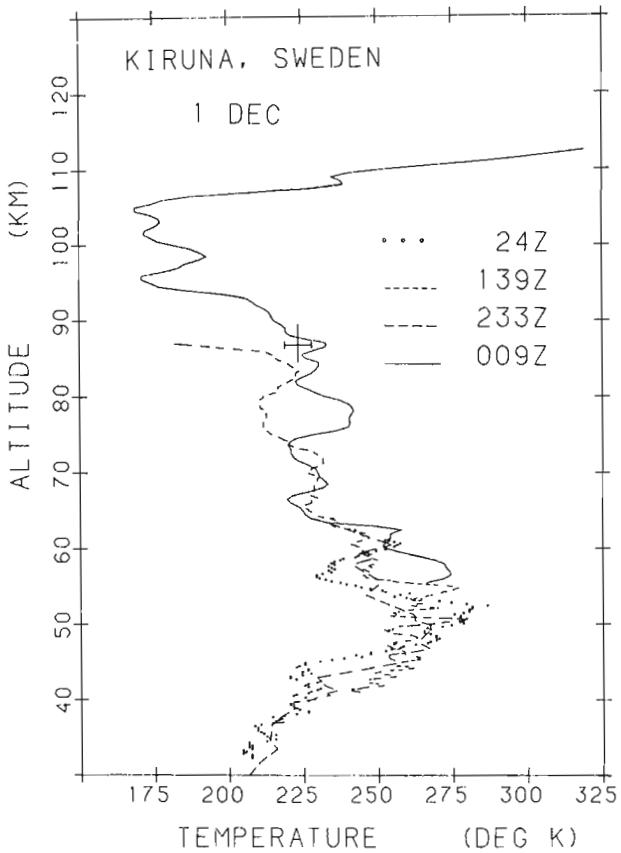

(b)

Fig. 5. The measurements of temperatures are shown for (a) salvo B and (b) salvo A2 for datasonde, passive sphere, accelerometer sphere, mass spectrometer and infrared spectrometer techniques. All of the profiles were measured at Esrange, Sweden, except the mass spectrometer profile which was measured at Andøya, Norway. The large irregular features in the 90–110 km region in salvo B may be associated with acoustical waves.

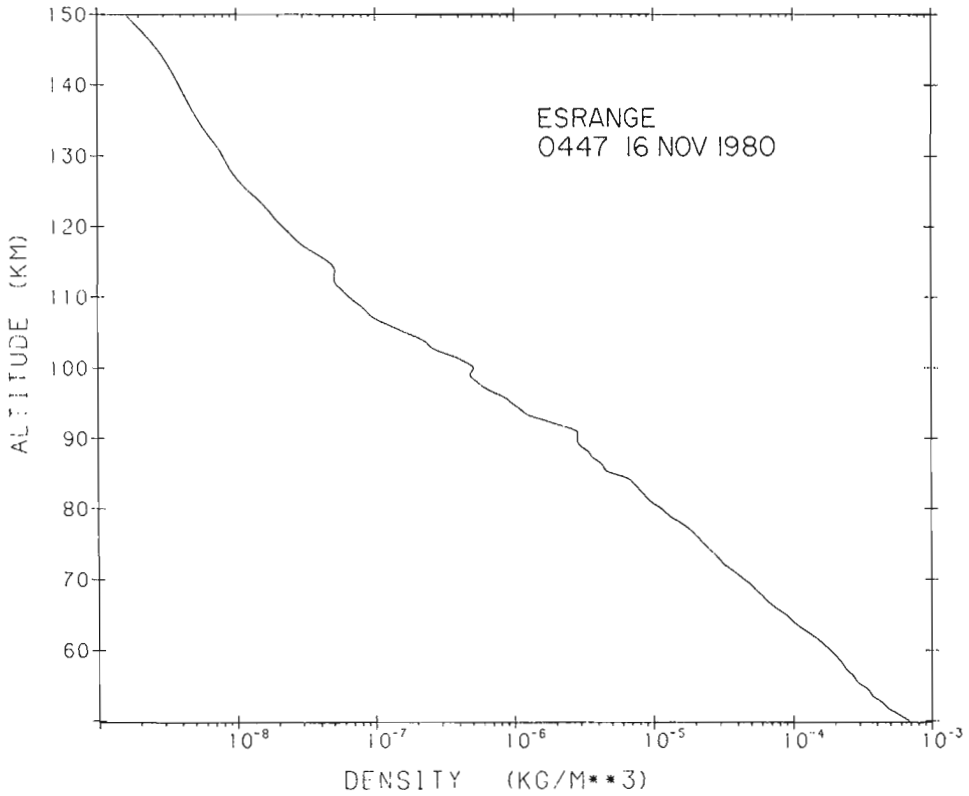

Fig. 6. The density profile measured during salvo B by the piezoelectric accelerometer technique is shown between 50 and 150 km. The features observed at 112, 100 and 90 km indicate a strongly perturbed atmosphere which must have a very strong localized temperature structure (as indicated in Fig. 5) or, more likely, indicate the presence of acoustical waves.

layer. The evidence has led to the conclusion that these features could be associated with aurorally generated shock waves. The morning of salvo B was moderately active in terms of geomagnetic activity and extremely active in terms of auroral activity which was present during the time period. The generation of shock waves by Joule heating and Lorentz coupling in the auroral electrojet region has been studied by several investigators (WILSON, 1967; WILSON, 1969; PROCUNIER, 1971; WILSON 1972; CHIMONAS, 1977). The studies of auroral shock waves and transmission of infrasound signatures has been developed and tested by several of these investigators. Typical strength of the shock waves discussed in these studies are 1–10 dynes cm^{-2} and the lower atmosphere does not significantly attenuate the amplitude of the wave for frequencies less than 1 Hz. For reference it should be remembered that the pressure of 1 dyne cm^{-2} corresponds to an altitude near 93 km. From the prior investigations a typical velocity was in the vicinity of 500 to 600 m s^{-1}. A normal shock wave corresponding to a Mach number of 1.5 would have a pressure ratio of about 3, a density ratio of about 2 and a temperature ratio of about 1.4. The observed features would be consistent with density measurement in the region of a shock wave and the likelihood that such a condition could exist during this experiment is high. At Esrange the sky was overcast during the salvo B launch period and thus no auroral pictures exist which could substantiate the presence of fast moving auroral forms. However, at Andøya Rocket Range the sky was clear and very active conditions were seen to exist. Bright auroral forms were observed which showed rapid movement over Andøya during the entire salvo B period. The Andøya records also showed the presence of strong aurora over Esrange at 0450Z, when the accelerometer payload was flying, but at an elevation of 26° (the 100 km altitude range of the rocket trajectory) it is not possible to discern any motion due to edge view distortion. The temperature profiles shown for salvo B must be regarded with some caution (the region around the three features in the profile of Fig. 6), because it is uncertain if the error in temperature would be substantially increased by the departures from hydrostatic equilibrium which would accompany the pressure pulse of an aurorally generated shock wave.

In conclusion, the wave structure observed in the middle and upper atmosphere during the Energy Budget Campaign, high latitude winter conditions,

shows that the region is in a highly active dynamical state. The comparisons indicate that the geomagnetic storm conditions are most likely responsible for the increased temperatures in the 110–140 km region and may have been associated with the enhanced wave activity during salvoes B, Al and A2. The changes in the stratospheric and mesospheric temperature profiles between salvoes B and A1 could have been associated with a change in the circulation pattern over the northern hemisphere, LABITZKE and BARNETT (1985). The strong perturbations observed during salvo B may be due to the presence of aurorally generated shock or internal waves radiating from the edge of a moving auroral form.

Acknowledgements—The authors gratefully acknowledge the efforts of the launch support teams of Esrange, Andøya Range, DFVLR and NASA Wallops, whose outstanding efforts contributed substantially to the accomplishments of this program. In particular, the efforts of XAVIER KALTEIS and the DFVLR radar personnel contributed to the passive sphere results. The support provided by the Bundesminister fur Forschung und Technologie is acknowledged. Part of this work was accomplished while one of us (CRP) was visiting scientist at the Max-Planck-Institut for Kernphysik. The efforts of M. E. GARDNER and K. H. BHAVNANI in the analysis of the data are gratefully acknowledged.

REFERENCES

BAKER D. J., STEED A. J., WARE G. A., BARTSCHI B. Y. and STAIR A. T. JR — 1981 — Energy Budget Campaign 1980 Experiment Summary, BMFT-FB-W 81-052, p. 11. Bundesministerium für Forschung und Technologie, Bonn, F.R.G.

BAILERY A. B. and HIATT J. — 1972 — *AIA Aerospace* **10,** 1436.

CHIMONAS G. — 1977 — *J. geophys. Res.* **82,** 3573.

COESA — 1976 — *U.S. Standard Atmosphere, 1976.*

COLE K. D. — 1971 — *Planet. Space Sci.* **19,** 59.

COLE A. E. and KANTOR A. J. — 1978 — Air Force Reference Atmospheres, AFGL-TR-78-0051.

ENGLER N. A. — 1965 — Development of Methods to Determine Winds, Density, Pressure and Temperature from the ROBIN Falling Balloon, AFCRL-TR-65-448.

HINES C. O. — 1974 — *The Upper Atmosphere in Motion*, Am. Geophys. Un. Monograph 18.

KUMER J. B. — 1977 — *J. geophys. Res.* **82,** 2195.

LABITZKE K. and BARNETT J. J. — 1985 — *J. atmos. terr. Phys.* **47,** 173.

LANGE G., GERNDT R., TRINKS H. and OFFERMANN D. — 1981 — Energy Budget Campaign 1980 Experiment Summary, BMFT-FB-W 81-052, p. 11. Bundesministerium für Forschung und Technologie, Bonn, F.R.G.

MCCLATCHEY R. A., BENEDICT W. S., CLOUGH S. A., BURCH D. E., CALFEE R. F., FOX K., ROTHMAN L. S. and GARING J. S. — 1973 — AFCRL Atmospheric Absorption Line Parameters Compilation, AFCRL-TR-73-0096.

OFFERMANN D. — 1985 — *J. atmos. terr. Phys.* **47,** 1.

OFFERMANN D. and THRANE E. — 1981 — Energy Budget Campaign 1980 Experiment Summary, BMFT-FB-W 81-052, p. 11. Bundesministerium für Forschung und Technologie, Bonn, F.R.G.

PHILBRICK C. R., MCISAAC J. P. and FAUCHER G. A. — 1977 — *Cospar Space Res.* **17,** 349.

PHILBRICK C. R., FAIRE A. C. and FRYKLUND D. H. — 1978a — Measurements of Atmospheric Density at Kwajalein Atoll, 18 May 1977, AFGL-TR-78-0058.

PHILBRICK C. R., NOONAN J. P., FLETCHER E.T., JR, HANRAHAN T., SALAH J. E., BLOOD D. W., OLSEN R. O. and KENNEDY B. W. — 1978b — Atmospheric Properties from Measurements at Kwajalein Atoll on 5 April, AFGL-TR-78-0195.

PHILBRICK C. R., MCISAAC J. P., FRYKLUND D. H. and BUCK R. F. — 1981 — Energy Budget Campaign 1980 Experiment Summary, BMFT-FB-W 81-052, p. 11. Bundesministerium für Forschung und Technologie, Bonn, F.R.G.

PHILBRICK C. R., GROSSMANN K. U., HENNIG R., LANGE G., KRANKOWSKY D., OFFERMANN D., SCHMIDLIN F. J. and VON ZAHN U. — 1983 — *Adv. Space Res.* **2,** 121.

PROCUNIER R. W. — 1971 — *Geophys. J. R. astr. Soc.* **26,** 183.

QUIROZ R. S. and GELMAN M. — 1976 — *J. geophys. Res.* **81,** 406.

ROTHMAN L. S. — 1981 — *Appl. Opt.* **20,** 791.

SCHMIDLIN F. J. — 1981 — *J. geophys. Res.* **86,** 9599.

TORKAR K. M., URBAN A., BJORDAL J., LUNDBLAD J. Å., SØRAAS F., SMITH L. G., DUMBS A., GRANDAL B., ULWICK J. C. and VANCOUR R. P. — 1985 — *J. atmos. terr. Phys.* **47,** 61.

TRINKS H., MAYR H. G. and PHILBRICK C. R. — 1979 — *J. geophys. Res.* **83,** 1641.

WILSON C. R. — 1967 — *Nature* **216,** 131.

WILSON C. R. 1969 *J. geophys. Res.* **74,** 1812.
WILSON C. R. 1972 *J. geophys. Res.* **77,** 1820.
WIRTH J. and VON ZAHN U. 1981 Energy Budget Campaign 1980 Experiment Summary, BMFT-FB-W 81-052, p. 11. Bundesministerium für Forschung und Technologie, Bonn, F.R.G.